JGR Atmospheres

RESEARCH ARTICLE
10.1029/2022JD038041

Key Points:

- Balloon-borne measurements are used to build a northern hemisphere (NH) midlatitude climatology of stratospheric aerosol number density and size
- Variability of NH midlatitude stratospheric aerosol number density exhibits a minimum of a factor of ~2 near 22 km altitude ($\theta = 550$ K)
- NH Stratospheric aerosol perturbations during 2019–2022 are detected and characterized using aerosol microphysical properties

Supporting Information:

Supporting Information may be found in the online version of this article.

Correspondence to:

E. Asher,
Elizabeth.Asher@noaa.gov

Citation:

Todt, M. A., Asher, E., Hall, E., Cullis, P., Jordan, A., Xiong, K., et al. (2023). Baseline Balloon Stratospheric Aerosol Profiles (B^2SAP)—Systematic measurements of aerosol number density and size. *Journal of Geophysical Research: Atmospheres*, *128*, e2022JD038041. https://doi.org/10.1029/2022JD038041

Received 18 OCT 2022
Accepted 22 MAY 2023

Author Contributions:

Conceptualization: Michael A. Todt, Elizabeth Asher, Troy Thornberry
Data curation: Michael A. Todt, Elizabeth Asher, Emrys Hall, Patrick Cullis, Kensy Xiong
Formal analysis: Michael A. Todt
Funding acquisition: Troy Thornberry
Investigation: Michael A. Todt, Elizabeth Asher
Methodology: Michael A. Todt
Project Administration: Troy Thornberry
Resources: Troy Thornberry
Software: Allen Jordan
Supervision: Elizabeth Asher, Dale F. Hurst, Troy Thornberry
Validation: Michael A. Todt

Baseline Balloon Stratospheric Aerosol Profiles (B^2SAP)—Systematic Measurements of Aerosol Number Density and Size

Michael A. Todt[1,2,3], Elizabeth Asher[1,2], Emrys Hall[1,4], Patrick Cullis[1,4], Allen Jordan[1,4], Kensy Xiong[1,4], Dale F. Hurst[1,4], and Troy Thornberry[2]

[1]Cooperative Institute for Research in Environmental Sciences (CIRES), University of Colorado, Boulder, CO, USA, [2]Chemical Sciences Laboratory, National Oceanic and Atmospheric Administration (NOAA), Boulder, CO, USA, [3]Now at Finnish Meteorological Institute (FMI), Helsinki, Finland, [4]Global Monitoring Laboratory, National Oceanic and Atmospheric Administration (NOAA), Boulder, CO, USA

Abstract Stratospheric aerosol plays an important role in Earth's radiative balance. Systematic measurements of stratospheric aerosol number concentration and size are needed to characterize their baseline values and variability, improve understanding of aerosol microphysics, and assess the representation of stratospheric aerosol processes in global models. In situ measurements of particle size distribution provide insight into the responses of stratospheric aerosol processes to perturbations from volcanoes and wildfires, anthropogenic emissions from rockets and aircraft, or intentional injections related to climate intervention. The Baseline Balloon Stratospheric Aerosol Profiles (B^2SAP) project uses compact, lightweight payloads carried by meteorological balloons to measure aerosol number density and size distributions, water vapor, ozone, and meteorological data from the surface to the middle stratosphere. The long-term goal for the B^2SAP project is to produce climatologies of aerosol number and size distributions into the middle stratosphere at latitudinally distributed measurement sites. Since March 2019, B^2SAP payloads have been launched from Boulder, CO, USA once to twice per month and four to six times per year from Lauder, NZ. These measurements provide a new record of in situ stratospheric aerosol observations and are being used to help validate satellite-based estimates of stratospheric aerosol size distributions. Here we present 50 vertical profiles from Boulder, CO, from March 2019 to March 2022, to build a NH mid-latitude climatology of stratospheric aerosol and its variability and investigate the impact of natural perturbations on stratospheric aerosol microphysics.

Plain Language Summary Particles in the stratosphere play important roles in chemistry and climate. Lightweight instruments carried by weather balloons can provide systematic measurements of the particle number and size, atmospheric water vapor and ozone (two gases that also influence atmospheric chemistry and climate) to inform these areas of research. Without weather in the stratosphere, the sources and sinks of particles are few, and concentrations of particles change slowly over time, in the absence of powerful volcanic eruptions or large wildfires, which can inject or loft material into the stratosphere. Particularly in these cases, balloon-borne observations can be critical to validating satellite retrievals and improving global climate models. As part of the Baseline Balloon Stratospheric Aerosol Profiles (B^2SAP) project, weather balloon launches with the instruments described above have taken place from Boulder, CO, USA and Lauder, NZ since March 2019. Here we present 50 vertical profiles from Boulder, CO from March 2019 to March 2022, which are used to provide a new record (to produce a climatology) at midlatitudes in the in the northern hemisphere and investigate the impact of volcanic eruptions and large wildfires within this period.

1. Introduction

Aerosol particles in the stratosphere, including those initially described by Junge and colleagues (Chagnon & Junge, 1961; Junge et al., 1961; Junge & Manson, 1961), have an important and variable influence on Earth's radiation budget. These particles scatter incoming solar radiation, some of which is reflected back to space, cooling the planet (IPCC et al., 2021; Kremser et al., 2016; Robock, 2000; Solomon et al., 2011). For example, in the two years following the eruption of Mt. Pinatubo in 1991, the stratospheric aerosol enhancement decreased the global average surface temperature by 0.5°C (e.g., Dutton & Christy, 1992; Grainger et al., 1995; Hansen et al., 1996; Hervig & Deshler, 2002; Massie et al., 1996; Russell et al., 1996; Thomason et al., 1997).

Visualization: Michael A. Todt
Writing – original draft: Michael A. Todt
Writing – review & editing: Elizabeth Asher, Emrys Hall, Patrick Cullis, Kensy Xiong, Dale F. Hurst, Troy Thornberry

Quantifying stratospheric aerosol radiative properties is critical to reducing the uncertainty in radiative forcing in climate models (Bellouin et al., 2020; Carslaw et al., 2013). Aerosol abundance and size distributions determine aerosol cross sections and surface area densities, which are critical parameters for model representations of aerosol radiative forcing (e.g., Murphy et al., 2021) and stratospheric heterogeneous chemistry (Deshler et al., 1996; Fahey et al., 1993; Hofmann & Solomon, 1989; Jäger & Wege, 1990; Solomon et al., 1996). High quality, long-term aerosol size and number distribution measurements provide important information for both these representations.

Systematic measurements of stratospheric aerosol provide insight into drivers of variability in stratospheric aerosol abundance and microphysics, such as the introduction and evolution of aerosols from large perturbation events, like volcanic eruptions and plumes from intense wildfires that reach the stratosphere. They also provide information on aerosol processes that can be used to improve representations in models. Better understanding of stratospheric aerosol processes is needed to predict the impacts of potential climate intervention (CI) using stratospheric aerosol injection (SAI). A sustained program of routine measurements could also be used for sensitive detection and characterization of future efforts at CI.

Past in situ optical particle counter (OPC) measurements of stratospheric aerosol span four decades at a range of sites for particles with diameter >0.30 μm and <20 μm (Hofmann et al., 1975; Deshler et al., 1996, 2003, 2019; Kalnajs & Deshler, 2022; and references therein), with most of the data taken at northern hemisphere (NH) midlatitudes, in particular from Laramie, Wyoming. During this period, OPCs underwent a series of improvements, including a shift from white–light to laser light sources, accompanied by higher instrument flow rates, and an increase in the number of size bins from 2–4 in 1971 to 8 after 1989. These changes improved measurement accuracy and precision and expanded the range of detectable particle size acheivable with OPCs from >0.35 μm and <0.56 μm in 1971 to >0.30 μm and <9 μm in 2008. More recent improvements in aerosol measurement technology allow for higher size resolution measurements and the detection of smaller particles with OPC instruments that are sufficiently light to be carried to ∼28 km using small meteorological balloons.

In March 2019, monthly and quarterly balloon soundings were initiated from Boulder, Colorado (39.9° N, 105.2° W), and Lauder, New Zealand (45.1° S, 169.7° E), respectively, to validate retrievals of stratospheric aerosol properties by the third generation Stratospheric Aerosol and Gas Experiment on the International Space Station (SAGE III-ISS) with Portable Optical Particle Spectrometer (POPS) measurements of aerosol number density and size distributions (Gao et al., 2016). Simultaneous balloon-borne measurements using ozonesondes and frost point hygrometers at both sites also support the validation of SAGE III-ISS retrievals of ozone and water vapor (Davis et al., 2021; Wang et al., 2020). In June 2020, the frequency of POPS sonde launches at Boulder was increased with the initiation of the Balloon Baseline Stratospheric Aerosol Profiles (B^2SAP) project to accumulate additional baseline measurements as part of NOAA's Earth's Radiation Budget (ERB) program. B^2SAP added two quarterly launch sites in 2022 in the NH and Southern Hemisphere (SH) tropics: Hilo, Hawaii, and the Maïdo Observatory on La Réunion. A subset of B^2SAP launches from Boulder and Lauder, New Zealand are still scheduled to coincide with SAGE III-ISS overpasses to support continued satellite retrieval validation.

2. Methods

2.1. Sondes

From March 2019 to March 2022, 50 successful balloon soundings were carried out from Boulder, CO (39.9°N, 105.2°W), initially on a roughly monthly basis, then increasing to twice-monthly in June 2020. In addition to the POPS (Handix Scientific, Inc., Fort Collins, CO), B^2SAP payloads include an electrochemical concentration cell (ECC) ozonesonde (Environmental Science; Sterling et al., 2017 and references therein), a NOAA Frost Point Hygrometer (FPH; Hall et al., 2016) and an iMET-1 (InterMet Systems) radiosonde for data telemetry to a ground-based receiving system at 1–2 s intervals.

B^2SAP sonde flights reach altitudes of up to 28 km. Valved balloons are used (Hall et al., 2016; Krauchi et al., 2016) to achieve payload descent speeds similar to ascent speeds (∼5 m/s), and as a result, measurements made during ascent and descent are of the same vertical resolution, and for the FPH and POPS, comparable quality. For soundings where POPS data collection did not continue at least 10 km into the descent, only ascent data is used.

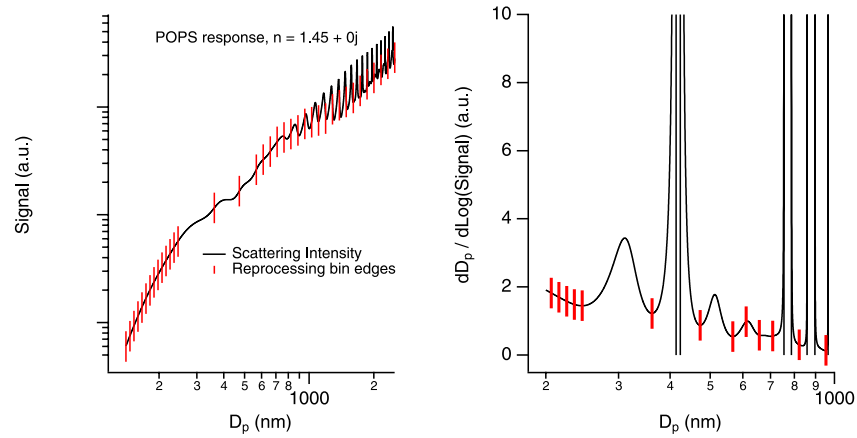

Figure 1. (a) Simulated POPS scattering response (black line) shows strong Mie oscillations starting around 0.300 nm in diameter. Red lines indicate bin edges for our non-uniform 36 bin scheme, avoiding flat or non-monotonic regions between 250 and 600 nm. (b) $dD_p/dLog(Signal)$ in the range of 0.20–1.0 μm in diameter, illustrating the placement of bin edges to avoid regions with large changes in size for relatively small changes in scattering signal.

2.2. POPS Size Binning

POPS is a compact, lightweight light scattering optical particle spectrometer orginally developed at NOAA (Gao et al., 2016) capable of detecting and sizing particles in a diameter size range of 140–2,500 nm. How a particle scatters light is a function of its size, shape and refractive index (RI). In an optical particle sizing instrument, assuming an accurate RI is critical for accurate particle size determination (Quenzel, 1969). In the stratosphere, where sulfuric acid particles dominate (Froyd et al., 2009; Murphy et al., 2021; Rollins et al., 2018), we use a constant RI of $n = 1.45 + 0j$, the index of refraction of pure sulfuric acid (Russell & Hamill, 1984; Russell et al., 1996; Steele & Hamill, 1981) at 405 nm, the wavelength of the POPS laser. Contributions to the aerosol population from mixed organic-sulfate aerosol are expected, especially near the tropopause, and a subset of the sulfuric acid particles contain meteoric material (Murphy et al., 2021). Reliable values for the RI of secondary organic aerosol in the upper troposphere, lower stratosphere (Li et al., 2021) and aerosol meteoric material containing aerosol are less well constrained. To illustrate the uncertainty introduced by differences from the assumed value, if the true RI is $n = 1.61 + 0j$ (an extreme case) the POPS measured size range would shift from 140–2,500 nm to 125–2,253 nm. A non-zero imaginary component of RI, such as in a particle containing black carbon, would have an even larger impact on particle sizing. For the measurments presented here, this uncertainty is likely largest in the troposphere, and less influential in the stratosphere, where the major component is typically sulfuric acid. Exceptions to this are where stratospheric aerosol are volcanic ash, containing rock and minerals, or wildfire smoke, which is largely composed of organic aerosol and black carbon.

In the particle size range measured by the POPS, light scattering is generally proportional to particle diameter, although not monotonically due to the presence of Mie oscillations that affect size determination at various diameters. This is apparent in the POPS signal Mie scattering calculation shown in Figure 1a. To reduce the impact of this uncertainty, we have avoided locating bin edges at particle diameters where small changes in scattering intensity correspond to large changes in diameter (i.e., $dD_p/dSignal$ is large) or where non-monotonic Mie oscillations exist, as shown in Figure 1b. For this reason, size distributions are not normally distributed in Log-diameter space throughout (Figure 1). At sizes below 0.25 μm in diameter, there is a monotonic relationship between aerosol size and signal, and size bins are evenly spaced on a log scale. From 0.25 to 0.600 nm, bin edges are placed at minima in $dD_p/dSignal$ to confine non-monotonic portions of the Mie curve within individual bins. Beyond 600 nm, when the size and shape of Mie oscillations overwhelm other sources of uncertainty, evenly spaced log D_p bins are resumed. With the typical balloon payload including an iMET-1, POPS, FPH, and ECC ozonesonde, the available radiosonde telemetry bandwidth for POPS data limits the transmitted size distribution resolution to 15 bins. When payloads are recovered, we reprocess the recorded single particle data into a higher number of size bins using the theoretical scattering response of particles at a selected value of the RI. All data presented here have been reprocessed into 36 size bins (Figure 1a) using an assumed RI of $n = 1.45 + 0j$. As noted above, uncertainty in particle size increases in cases where the assumed RI is inaccurate. A more accurate assumption for RI in air

masses heavily influenced by either pyrocumulonimbus (PyroCB) or ash-rich volcanic plumes would require a tailored binning scheme (and a good understanding of the aerosol composition) to reduce the uncertainty in size determination. In this study, all flights have been analyzed consistently due to rare and uncertain contributions from PyroCB (and no known emissions of ash-rich volcanic aerosol) during this period in the NH midlatitudes.

2.3. Stratospheric POPS Measurements

To improve instrument performance at the low ambient pressures at high altitude, modifications have been made to the original POPS design presented by Gao et al. (2016) and subsequently incorporated into all POPS currently produced. Chamber tests demonstrated that for atmospheric pressures below ~200 hPa in the original design, the particle velocity through the laser beam decreased, due to the expansion of the sample jet. At pressures below ~60 hPa, the sample jet divergence became wide enough that some particles passed through the edge of the laser beam, producing artificially low scattered light intensities and resulting in the under-sizing and undercounting of particles. To mitigate this issue for stratospheric measurements, the POPS sample chamber exit port was redesigned to mirror the smaller diameter inlet nozzle and the gap between the inlet nozzle and exit port was narrowed to constrain the divergence of the sample jet (Figure S1 in Supporting Information S1). Additionally, the sample and sheath flows were increased with decreasing pressure to compensate for the otherwise observed decrease in particle velocity. At ground level pressure (~830 mb in Boulder), the sample flow rate is set to 3 $cm^3\ s^{-1}$ and is then increased in a series of ambient pressure-based flow steps starting at 200 hPa up to a rate of ≥5.5 $cm^3\ s^{-1}$ (the sheath flow scales accordingly) to maintain a sufficient mass of air at lower pressures. Extensive laboratory pressure chamber tests of POPS instruments modified and operated as described above determined that the modified POPS (Figure S1 in Supporting Information S1) accurately counts and sizes particles at pressures at or above 20 hPa when the sample flow is at least 3.0 $cm^3\ s^{-1}$. At pressures below ~25 hPa the POPS miniature rotary vane pump (Thomas G 6/01-K-LCL) typically ceases to be capable of maintaining a sufficient (3 $cm^3\ s^{-1}$) sample flow rate through the instrument for measurement consistency. Data points where the POPS sample flow rate (before temperature correction has been performed) drops below 3 $cm^3\ s^{-1}$ are flagged in data processing and have been excluded from the analysis shown here (Figure S2 in Supporting Information S1).

Particle concentration (cm^{-3}) is calculated by dividing the particle counts within a size range of interest by the temperature-corrected instrument sample flow rate ($cm^{-3}\ s^{-1}$). Sample flow rates (and temperatures) reported in the telemetered data product are corrected in data processing to account for the difference between the ambient temperature, measured by a radiosonde, and the temperature of the POPS laminar flow element (measuring the volumetric sample flow) to yield the temperature corrected instrument flow rate described above (Figure S2 in Supporting Information S1). Particle concentration uncertainty is dominated by precise knowledge of the sample flow rate, which is calibrated to better than 5% (Gao et al., 2016).

For balloon-borne payloads, the POPS is housed in a thermally insulating foam box to maintain an operating temperature between −5 and 35°C. The box is also electronically shielded with aluminum foil to reduce electronic noise and RF interference from radiosonde telemetry. Particles dry out during sampling because the sample flow heats up as it passes through tubing enclosed in the insulated foam box prior to detection. Temperature differences can be as high as 60°C. However, relative humidity (RH) in the stratosphere is typically very low, and differences between dry and ambient particle size due to changes in temperature can be ignored as they are likely below the inherent size uncertainty of ~3% at 500 nm (Gao et al., 2016), assuming the correct selection of RI as discussed above. In the coarse mode, above ~600 nm in diameter, Mie oscillations introduce uncertainty in sizing over 15%.

2.4. Measurement Consistency

To demonstrate inter-instrument measurement consistency, two POPS were launched <5 min apart on separate balloons. Figure 2a shows the total aerosol concentration profiles from each instrument. Both balloons (A and B) followed a similar flight trajectory. Total number concentrations from the near-simultaneous flights are similar, with median concentrations and interquartile ranges (shaded regions) per altitude bin overlapping for the duration of the flights. Larger relative differences in particle concentration occurred at altitudes of low particle concentration. Differences within individual size bins largely remain <30%; larger differences are observed at large Dp, where POPS counting statistics are poor under baseline conditions (Figure 2c). Consistency between instruments provides confidence in the body of data collected using the suite of similar instruments launched over the course

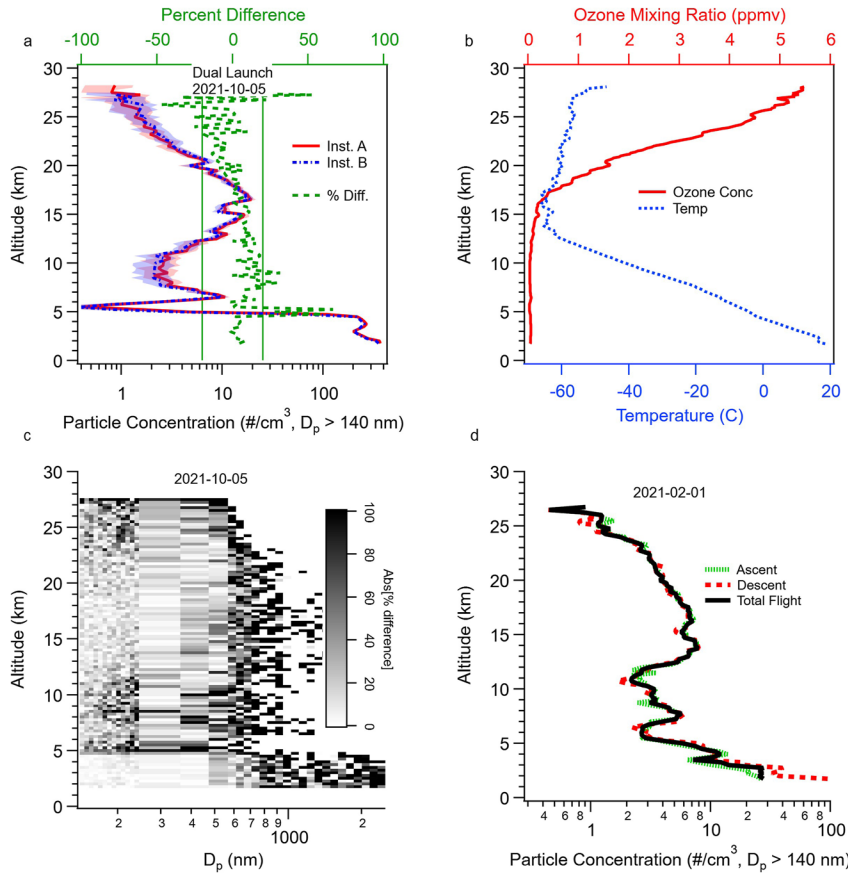

Figure 2. (a) Profiles of median particle concentrations from two POPS launched on separate balloon payloads within 5 min of each other on 5 October 2021. Shaded regions are the inner quartile range (IQR) of individual POPS measurements, and vertical green lines indicate ±20 percent difference in measured particle concentration between instruments. (b) Ozone mixing ratios (top axis, red line) and ambient temperature (bottom axis, blue lines) profiles from 5 October 2021. Temperature profiles from both balloon payloads are included, but are nearly identical. Ozone data from the second launch not available. (c) Percent difference between ascent and descent size distributions on 1 February 2021. Note that large differences are mainly seen in larger size bins, where particle counts are low (and counting statistics are poor). (d) Ascent (dotted green), descent (dashed red) and the mean ascent–descent (solid black) particle concentration profiles from 1 February 2021, demonstrating the consistency between ascent and descent profiles, when descent data are available.

of the 3-year period of the measurements presented. There is a high degree of confidence that flight-to-flight variations in aerosol concentration are attributable to changes in atmospheric conditions, not measurement error.

As mentioned above, the use of a valved balloon slows the descent speed to 5 m/s, which allows for high-quality measurements during both the ascent and descent. In general, the ascent and descent profiles are very similar (Figure 2c). When possible, ascent and descent data are used in analysis to improve counting statistics.

Prior to every flight, each POPS goes through a range of calibrations and performance checks. The detector gain is adjusted to produce a defined peak signal from 508 nm polystyrene latex spheres to ensure particle sizing is correct and consistent between instruments. The instrument sample flow calibration is checked regularly using a primary flow standard (Gilibrator-2 or mini-Buck Calibrator) to ensure particle concentration measurements are accurate. In addition, vacuum chamber tests are performed on each instrument before it is initially used on a launch to verify that its flow rate performance will maintain a flow of 3 cm^3 s^{-1} to ≤25 hPa. The detector baseline signal and its standard deviation are monitored to ensure instrument noise is not impacting aerosol counts in the smallest size bins.

3. Results and Discussion

POPS in situ measurements provide insight into stratospheric aerosol microphysics, for example, how size distributions and number concentration vary with altitude, with season, or as a function of time after a perturbation.

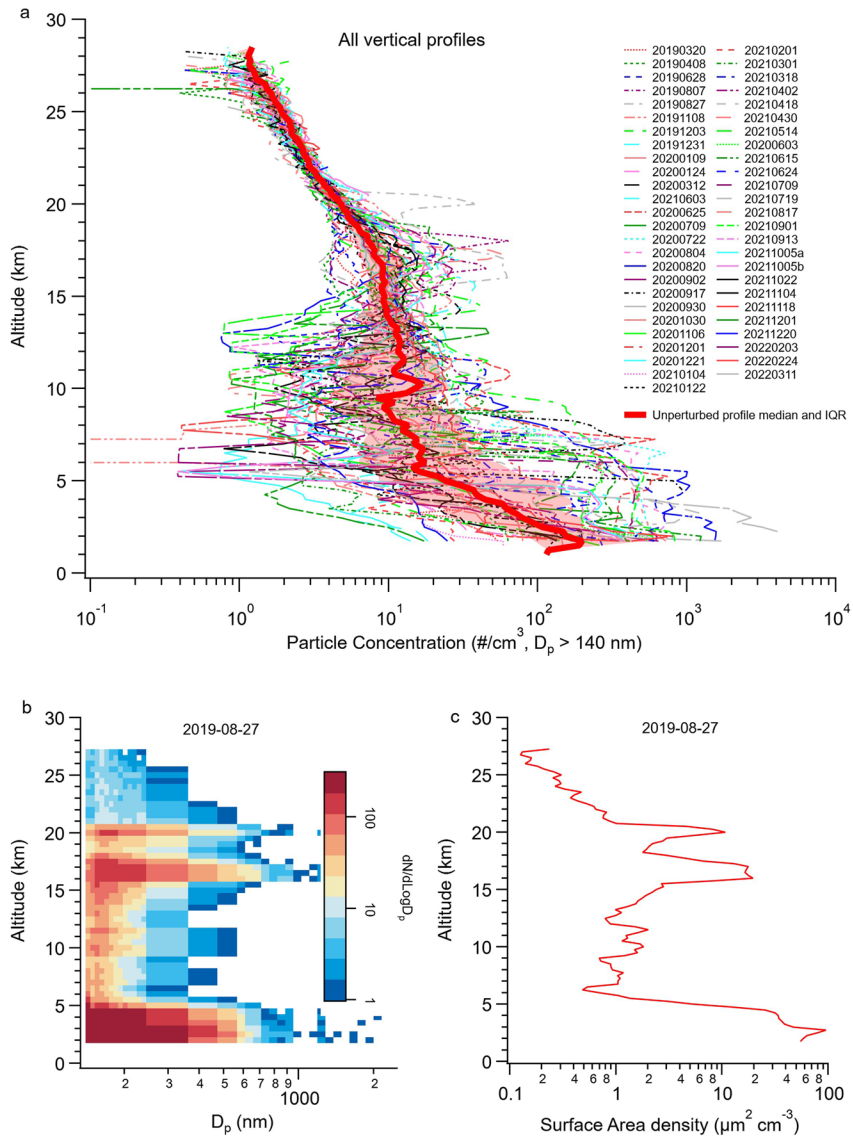

Figure 3. (a) All profiles collected from March 2019–March 2022. Altitude is reported by GPS, concentration is the median total concentration (D_p > 140 nm) from each 1s period within a given 250m altitude bin, using data reprocessed into the 36-bin scheme described in Section 2.3. The "unperturbed profile average" is the median of all 30 profiles without significant contributions from volcanic eruptions, with the IQR shown in the shaded region. (b) Altitude resolved particle size distribution from 27 August 2019. Green dashed line at 17 km highlights the portion of the altitude distribution used for the size distribution in Figure 5b, also shown as a green dashed line. (c) Surface area density calculated from the size distribution in (b).

Figure 3a shows 50 vertical profiles of aerosol concentrations for particles with diameters between 140 and 2,500 nm from flights between March 2019–March 2022. An example of the vertically resolved size distribution measurements from a POPS sonde profile in August 2019 is shown in Figure 3b, with the corresponding calculated total measured aerosol surface area density shown in Figure 3c. The "background" vertical profile shown in Figure 3a is the median of all profiles without detectable evidence of recent volcanic or pyrogenic perturbation, here meaning elevated aerosol concentration or surface area following known volcanic or pyroCB activity, such as is apparent in the layers near 17 km and 20 km in the profile shown in Figures 3b and 3c. In the absence of an obvious, strong perturbation, stratospheric aerosol concentrations in 250 m altitude bins are observed to vary by a factor of ~2–4. This variability is small compared to variations more than two orders of magnitude observed in the upper troposphere. In the event of a strong perturbation (e.g., a volcanic eruption) we have observed stratospheric aerosol concentrations elevated by an order of magnitude.

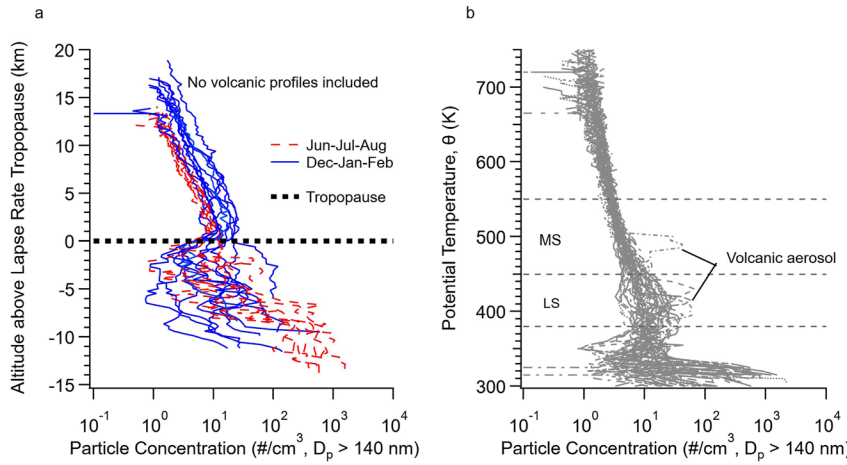

Figure 4. (a) Particle concentration versus. lapse rate tropopause height from Boulder, CO, USA. Profiles in December, January, or February are solid blue lines. Profiles in June, July, or August are dashed red lines. (b) Particle concentration versus potential temperature. Dashed black lines indicate the boundaries of the middle stratosphere (MS) and lower stratosphere (LS), as defined above.

The simultaneous measurements of pressure, temperature, relative humidity, water vapor and ozone from the same balloons as POPS sonde flights facilitate tracking perturbations, quantifying seasonal variation in stratospheric aerosol, and assessing its influence on stratospheric chemistry. Figure 4a shows the total aerosol concentration relative to the lapse rate tropopause (World Meteorological Organization, 1957) determined for each profile with no obvious influence from volcanic or wildfire activity. The tropopause demarcates a clear transition in aerosol concentration variability. At an altitude of 2 km above the tropopause, median particle concentration is 50% higher than 2 km below the tropopause, while the range in median concentration is an order of magnitude larger 2 km below the tropopause than 2 km above the tropopause. In addition, seasonal variability of stratospheric aerosol concentration relative to the tropopause has been previously reported, with increased aerosol concentration observed in winter compared to summer (*e.g.,* Barnes & Hofmann, 2001). Although we observed similar seasonal variation in our 3-year record (e.g., for non-perturbed profiles, the average concentration 2 km above the tropopause is 80% higher during the months of December-February than during June-August), these differences are mainly due to the height of the troposphere being lower in winter, rather than changes in aerosol concentration versus absolute altitude.

Stratospheric aerosol perturbations related to the eruptions of the Raikoke volcano (48.3°N, 153.2°E) in June 2019, which injected an estimated 1.5 Tg of SO_2 into the stratosphere (de Leeuw et al., 2021), and La Soufrière (13.3°N, 61.2°W) on the Caribbean island of St. Vincent in April 2021, which injected approximately 0.5 Tg of SO_2 (NASA Earth Observatory, 2021) are clearly visible in the aerosol profiles over Boulder (Figures 4b and 5). POPS measurements during unperturbed conditions exhibit less than an order of magnitude of variability in aerosol concentration in the lower stratosphere (LS, here defined as having potential temperature 380-450 K- Figure 4b), while in the middle stratosphere (MS, 450–550 K) aerosol concentration typically varies by less than a factor of three. Exceptions to this altitude dependence are profiles which encountered layers of elevated aerosol concentration up to 5 km above the tropopause that are related to volcanic activity. The profiles of particle concentration versus potential temperature plotted in Figure 4b show the consistency of aerosol concentration above 450 K, in the absence of a perturbation event such as a volcanic eruption.

Profiles from August to November 2019 and May to December 2021 provide two examples of the influence that moderate volcanic eruptions can have on the NH mid-latitude aerosol loading in the LS and MS. In the LS, profiles from August of 2019, which sampled the volcanic plume from Raikoke, reveal layers with up to a ten-fold increase in particle concentration compared to concentrations from a profile in June of 2019, prior to the arrival of the Raikoke plume over Boulder (Figure 5a). Particle concentrations in the LS over Boulder remained elevated through November of 2019. Similar to Raikoke, particle concentrations after the eruption of La Soufrière in 2021 were an order of magnitude higher than background levels in a thin layer. Elevated aerosol loading attributed to La Soufrière was first observed over Boulder on 30 April 2021, and persisted for 3–4 months, though calculated extinction was lower, for reasons discussed below.

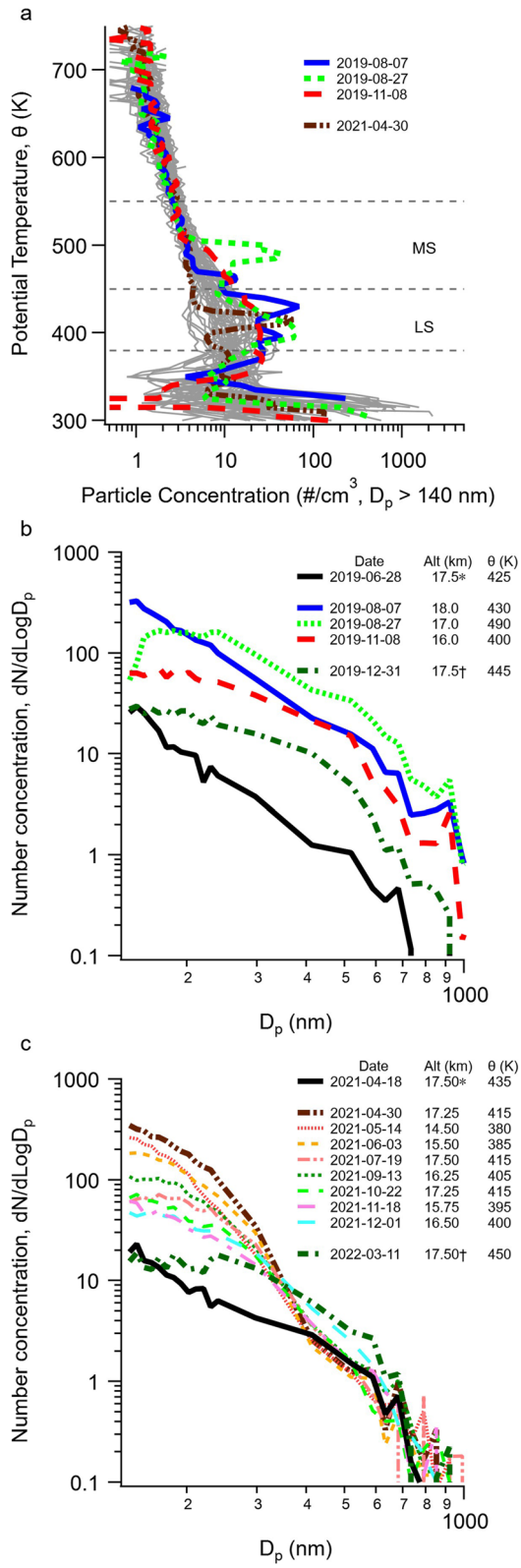
a
Potential Temperature, θ (K)
700
600
500
400
300
2019-08-07
2019-08-27
2019-11-08
2021-04-30
MS
LS
1
10
100
1000
Particle Concentration (#/cm3, Dp > 140 nm)
b
Number concentration, dN/dLogDp
1000
100
10
1
0.1
Date Alt (km) θ (K)
2019-06-28 17.5* 425
2019-08-07 18.0 430
2019-08-27 17.0 490
2019-11-08 16.0 400
2019-12-31 17.5† 445
2 3 4 5 6 7 8 9 1000
Dp (nm)
c
Number concentration, dN/dLogDp
1000
100
10
1
0.1
Date Alt (km) θ (K)
2021-04-18 17.50* 435
2021-04-30 17.25 415
2021-05-14 14.50 380
2021-06-03 15.50 385
2021-07-19 17.50 415
2021-09-13 16.25 405
2021-10-22 17.25 415
2021-11-18 15.75 395
2021-12-01 16.50 400
2022-03-11 17.50† 450
2 3 4 5 6 7 8 9 1000
Dp (nm)

Figure 5.

Vertically resolved size distributions also provide insight into the differences in aerosol characteristics from different volcanic eruptions. Figures 5b and 5c show aerosol size distributions at the stratospheric altitudes where maximum particle concentration was observed in individual profiles following volcanic eruptions. In these cases, we found distinct size distributions in individual altitude bins following the volcanic eruptions of Raikoke and La Soufrière. The eruption of Raikoke directly injected a greater mass of SO_2 into the atmosphere than that of La Soufrière, leading to an increase in the mode of the aerosol size distribution (from ∼150 to ∼170 nm for the 3 months after Raikoke) and elevated concentrations of particles with diameters ≤700 nm. Following the eruption of La Soufrière, an increase in particle number was observed at the small sizes (to diameters of <400 nm). Light scattering efficiency increases strongly with particle diameter from 100 to 600 nm (Murphy et al., 2021). Therefore, the aerosol extinction signal produced by the increase in particle number after the La Soufrière eruption was too small to observe due to other sources of variability (Figure 6).

Figure 6a shows the time series of calculated aerosol extinction in the LS and MS over Boulder for the period from March 2019 to March 2022. An enhancement in extinction in both the LS and MS by a factor of five was observed two months after the eruption of Raikoke. The increased LS aerosol extinction attributed to the Raikoke eruption decayed approximately exponentially over the course of ∼6 months, with an e-folding time of $\tau = 176 \pm 47$ days (mean ± standard deviation) from the observed maximum extinction. This timescale is similar to that observed across the NH (Boone et al., 2022). The increase in aerosol number and the shift of the size distribution to larger diameters both contributed to the large increase in calculated extinction from Raikoke. The shift in the size distribution will affect climate and atmospheric chemistry in different ways. While smaller particles yield greater surface area for heterogenous chemical reactions per unit mass, particles with larger diameters have greater light scattering mass efficiency and thus a greater cooling effect (Murphy et al., 2021). Slightly elevated stratospheric aerosol extinction was also observed in February 2022 over Boulder, although the source of the enhancement in stratospheric aerosol extinction has not yet been identified.

Many of the B^2SAP launches were timed to coincide in space (±5° latitude, and ±10° longitude) and time (±24 hr) with solar occultation aerosol extinction retrievals by the SAGE III-ISS instrument. As mentioned above, aerosol extinction is calculated from the POPS data using the measured size distribution and assumptions about the aerosol composition and optical properties. Aerosol optical extinction calculated from the measured POPS size distributions can be directly compared to SAGE III-ISS measurements for example, at a wavelength of 520 nm. From vertically resolved size distributions, such as shown in Figure 3b, the aerosol optical extinction coefficient (Campuzano Jost et al., 2016) is calculated using the original formulation of Bohren and Huffman (1998) with the 36-bin sizing scheme discussed above (Section 2.2). Comparisons between SAGE III-ISS retrievals and POPS calculated extinction are shown in Figures 6b and 6c for background conditions and in the fresh volcanic plume from Raikoke, respectively. In both cases, the extinction calculated from POPS align closely with SAGE III-ISS retrievals, however, small differences exist in the plume altitudes (Figure 6c), likely due to the differences in the vertical and horizontal resolution, as well as the timing, of sonde and SAGE III-ISS observations.

Slightly increased extinction also occurred following the May 2020–November 2020 period of abnormally intense wildfire activity in Colorado and elsewhere in the western USA (May 2020–November 2020). Smoke from the Colorado fires was observed over 9,000 km away from Colorado (Baars et al., 2021). Stratospheric aerosol loading following large burning events is well documented, with aerosol carried into the stratosphere having lifetimes on the order of months (Fromm et al., 2010; Peterson et al., 2018; Yu et al., 2019). As noted above (Section 2.2) all sizing and extinction calculations shown here reflect an RI corresponding to sulfuric acid particles. Future work will address how changes in stratospheric aerosol composition related to wildfire smoke impact the uncertainty in aerosol sizing and calculated extinction.

High resolution size distributions enable the precise determination of aerosol surface area density, an important factor in stratospheric heterogenous chemistry. An example of the size resolution of reprocessed POPS data is shown in Figure 3b, along with the surface area profile (Figure 3c). Depending on the location and other atmospheric conditions, increased aerosol surface area can decrease ozone destruction by acting as a sink for active

Figure 5. (a) Highlighted vertical profiles show elevated stratospheric aerosol concentration following the eruption of Raikoke in June 2019 compared to "baseline" profiles in gray. (b) Size distributions from volcanic plumes at altitude of maximum particle concentration for launches showing elevated particle levels following the eruption of Raikoke. (c) Size distributions from volcanic plumes at altitude of maximum particle concentration for launches showing elevated particle levels following the eruption of La Soufrière. *Denotes profiles prior to observation of elevated aerosol concentrations due to volcanic activity. †Denotes profiles where aerosol contributions from volcanic activity has returned to "background" levels.

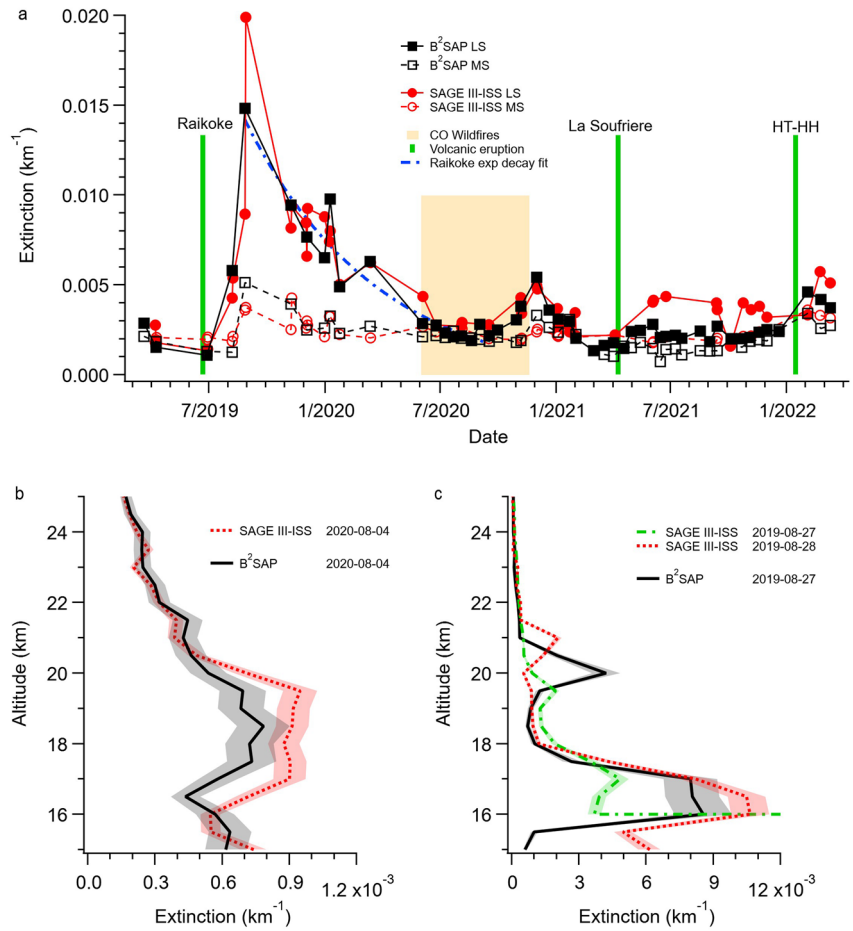

Figure 6. All extinction retrievals and calculations are for a wavelength of 520 nm. (a) POPS calculated aerosol extinction (red solid and dashed lines) and coincident SAGE III-ISS extinction retrievals (black solid and dashed lines) over Boulder in the LS and MS, with the timing of volcanic eruptions in the NH (e.g., Raikoke and La Soufrière) and SH (e.g., Hunga Tonga–Hunga Ha'apai; HT-HH) as well as a period of US wildfire activity indicated. Matching potential temperature for SAGE III-ISS extinction profiles, used to calculate extinction in the LS and MS, respectively, were interpolated from B^{2}SAP profiles based on geometric altitude. (b) Extinction retrievals by SAGE III-ISS on 2020-08-04 (red dotted line) and calculated extinction from POPS size distributions on 2020-08-04 (solid black line) binned at 500 m altitude resolution. (c) Extinction retrievals by SAGE III-ISS on both 2019-08-27 and 2019-08-28 (green dot-dashed line and red dotted line respectively) and calculated extinction from POPS size distributions on 2019-08-27 (solid black line) binned at 500 m altitude resolution. Reported uncertainty for SAGE III-ISS extinction retrievals is 8% (shown as the shaded red and green areas in Figures 6b and 6c). The uncertainty in the POPS calculated extinction, related to particle sizing and the aerosol jet flow, is ≤15% (shown as the shaded black areas in Figures 6b and 6c).

nitrogen species (Fahey et al., 1993) or increase ozone destruction by activating halogen chemistry (Hofmann & Solomon, 1989; Solomon et al., 1996). The chemical composition of volcanic eruptions also influences stratospheric ozone. Halogen concentrations from eruptions play a large role and can change the net effect of aerosol on ozone levels (Hofmann & Solomon, 1989). Additional information on the composition of volcanic injections is needed to fully account for how stratospheric heterogenous chemistry rates may change with the increased aerosol surface area.

4. Conclusions

Routine B^{2}SAP project launches are creating a baseline record in the NH midlatitudes of stratospheric aerosol number concentration and size distribution, against which stratospheric aerosol loading from natural and/or anthropogenic perturbations can be quantified. Since 2019, we have observed enhanced particle concentrations on multiple occasions related to volcanic eruptions and wildfires, as well as seasonal variation in aerosol

concentrations relative to the tropopause. Monitoring the changes in aerosol concentration and size distribution over time has enabled us to characterize differences in aerosol microphysics and evolution. Periods of increased number concentration are clearly distinguishable from those with background aerosol populations. Particle size distributions in volcanic plumes from the eruption of Raikoke show a distinct increase in particle diameter compared to the background state. As a result of the combined increase in size and number concentration, aerosol extinction was also elevated.

In addition to the profiles discussed here from Boulder, CO, balloon sonde POPS measurements of stratospheric aerosol have been made four to six times per year from Lauder, New Zealand, since 2019 and from La Réunion and Hilo, Hawaii since 2022. Planned expansion of the B^2SAP project to sites spanning a broad range of latitudes in both the NH and SH aims to provide a more global data set with which to compare stratospheric perturbations and help improve atmospheric modeling and climate prediction. Data from this project will be made publicly available on a regular basis.

Data Availability Statement

POPS data is available as 1 Hz time series at https://csl.noaa.gov/projects/b2sap/data.html under the supporting data tab for this manuscript Corresponding ozone, water, and meteorological data from these ERB flights and many other soundings can be found at the NOAA GML data repository: https://gml.noaa.gov/aftp/data/ozwv/ in the "Ozonesonde" and "WaterVapor" directories.

Acknowledgments
This work was supported in part by the NOAA Cooperative Agreement with CIRES, NA17OAR4320101, the NOAA Earth's Radiation Budget (ERB) project, and the NASA Upper Atmosphere Composition Observations (UACO) program.

References

Baars, H., Radenz, M., Floutsi, A. A., Engelmann, R., Althausen, D., Heese, B., et al. (2021). Californian wildfire smoke over Europe: A first example of the aerosol observing capabilities of aeolus compared to ground-based lidar. *Geophysical Research Letters*, *48*(8), e2020GL092194. https://doi.org/10.1029/2020GL092194

Barnes, J. E., & Hofmann, D. J. (2001). Variability in the stratospheric background aerosol over Mauna Loa Observatory. *Geophysical Research Letters*, *28*(15), 2895–2898. https://doi.org/10.1029/2001GL013127

Bellouin, N., Quaas, J., Gryspeerdt, E., Kinne, S., Stier, P., Watson-Parris, D., et al. (2020). Bounding global aerosol radiative forcing of climate change. *Reviews of Geophysics*, *58*(1), e2019RG000660. https://doi.org/10.1029/2019RG000660

Bohren, C. F., & Huffman, D. R. (1998). Absorption and scattering of light by small particles. https://doi.org/10.1002/9783527618156

Boone, C. D., Bernath, P. F., Labelle, K., & Crouse, J. (2022). Stratospheric aerosol composition observed by the Atmospheric Chemistry Experiment following the 2019 Raikoke eruption. *Journal of Geophysical Research: Atmospheres*, *127*(18), e2022JD036600. https://doi.org/10.1029/2022JD036600

Campuzano Jost, P., Dunlea, E., Cubison, M., & Jimenez, J. (2016). Scattering/extinction calculator: January 12, 2023 (version 2.0) [Software]. Cahiers Ivoiriens de Recherche Economique et Sociale. http://cires1.colorado.edu/jimenez-group/software/SizeDist_Scat_Ext_Mie_JGroup_Nov_2016_v2_0.ipf

Carslaw, K., Lee, L., Reddington, C., Pringle, K. J., Rap, A., Forster, P. M., et al. (2013). Large contribution of natural aerosols to uncertainty in indirect forcing. *Nature*, *503*(7474), 67–71. https://doi.org/10.1038/nature12674

Chagnon, C. W., & Junge, C. E. (1961). The vertical distribution of sub-micron particles in the stratosphere. *Journal of Meteorology*, *18*(6), 746–752. https://doi.org/10.1175/1520-0469(1961)018<0746:TVDOSM>2.0.CO;2

Davis, S. M., Damadeo, R., Flittner, D., Rosenlof, K. H., Park, M., Randel, W. J., et al. (2021). Validation of SAGE III/ISS solar water vapor data with correlative satellite and balloon-borne measurements. *Journal of Geophysical Research: Atmospheres*, *126*(2), e2020JD033803. https://doi.org/10.1029/2020JD033803

de Leeuw, J., Schmidt, A., Witham, C. S., Theys, N., Taylor, I. A., Pope, R. J., et al. (2021). The 2019 Raikoke volcanic eruption- Part 1: Dispersion model simulation and satellite retrievals of volcanic sulfur dioxide. *Atmospheric Chemistry and Physics*, *21*(14), 10851–10879. https://doi.org/10.5194/acp-21-10851-2021

Deshler, T., Hervig, M. E., Hofmann, D. J., Rosen, J. M., & Liley, J. B. (2003). Thirty years of in situ stratospheric aerosol size distribution measurements from Laramie, Wyoming (41°N), using balloon-borne instruments. *Journal of Geophysical Research*, *108*, (D5), 4167. https://doi.org/10.1029/2002JD002514

Deshler, T., Johnson, B. J., Hofmann, D. J., & Nardi, B. (1996). Correlations between ozone loss and volcanic aerosol at latitudes below 14 km over McMurdo Station, Antarctica. *Geophysical Research Letters*, *23*(21), 2931–2934. https://doi.org/10.1029/96GL02819

Deshler, T., Luo, B., Kovilakam, M., Peter, T., & Kalnajs, L. E. (2019). Retrieval of aerosol size distributions from in situ particle counter measurements: Instrument counting efficiency and comparisons with satellite measurements. *Journal of Geophysical Research: Atmospheres*, *124*(9), 5058–5087. https://doi.org/10.1029/2018JD029558

Dutton, E. G., & Christy, J. R. (1992). Solar radiative forcing at selected locations and evidence for global lower tropospheric cooling following the eruptions of El Chichón and Pinatubo. *Geophysical Research Letters*, *19*(23), 2313–2316. https://doi.org/10.1029/92GL02495

Fahey, D. W., Kawa, S. R., Woodbridge, E. L., Tin, P., Wilson, J. C., Johnson, H. H., et al. (1993). *In situ* measurements constraining the role of sulphate aerosols in mid-latitude ozone depletion. *Nature*, *363*(6429), 509–514. https://doi.org/10.1038/363509a0

Fromm, M., Lindsey, D. T., Servranckx, R., Yue, G., Trickl, T., Sica, R., et al. (2010). The untold story of pyrocumulonimbus. *Bulletin America Meteorology Social*, *91*(9), 1193–1210. https://doi.org/10.1175/2010BAMS3004.1

Froyd, K. D., Murphy, D. M., Sanford, T. J., Thomson, D. S., Wilson, J. C., Pfister, L., & Lait, L. (2009). Aerosol composition of the tropical upper troposphere. *Atmospheric Chemistry and Physics*, *9*(13), 4363–4385. https://doi.org/10.5194/acp-9-4363-2009

Gao, R. S., Telg, H., McLaughlin, R. J., Ciciora, S. J., Watts, L. A., Richardson, M. S., et al. (2016). A light-weight, high-sensitivity particle spectrometer for PM2.5 aerosol measurements. *Aerosol Science and Technology*, *50*(1), 88–99. https://doi.org/10.1080/02786826.2015.1131809

Grainger, R. G., Lamber, A., Rodgers, C. D., Taylor, F. W., & Deshler, T. (1995). Stratospheric aerosol effective radius, surface area and volume estimated from infrared measurements. *Journal of Geophysical Research*, *100*(D8), 16507–16518. https://doi.org/10.1029/95JD00988

Hall, E. G., Jordan, A. F., Hurst, D. F., Oltmans, S. J., Vömel, H., Kühnreich, B., & Ebert, V. (2016). Advancements, measurement uncertainties, and recent comparisons of the NOAA frost point hygrometer. *Atmospheric Measurement Techniques*, *9*, 4295–4310. https://doi.org/10.5194/amt-9-4295-2016

Hansen, J., Ruedy, R., Sato, M., & Reynolds, R. (1996). Global surface air temperature in 1995: Return to pre-Pinatubo. *Geophysical Research Letters*, *23*(13), 1665–1668. https://doi.org/10.1029/96GL01040

Hervig, M., & Deshler, T. (2002). Evaluation of aerosol measurements from SAGE II, HALOE, and balloonborne optical particle counters. *Journal of Geophysical Research*, *107*(D3), 4031. https://doi.org/10.1029/2001JD000703

Hofmann, D. J., Rosen, J. M., Pepin, T. J., & Pinnick, R. G. (1975). Stratospheric aerosol measurements I: Time variations at northern midlatitudes. *Journal of the Atmospheric Sciences*, *32*(7), 1446–1456. https://doi.org/10.1175/1520-0469(1975)032<1446:SAMITV>2.0.CO;2

Hofmann, D. J., & Solomon, S. (1989). Ozone destruction through heterogeneous chemistry following the eruption of El Chichón. *Journal of Geophysical Research*, *94*(D4), 5029. https://doi.org/10.1029/JD094iD04p05029

IPCC, Forster, P., Storelvmo, T., Armour, K., Collins, W., Dufresne, J.-L., et al. (2021). The Earth's energy budget, climate feedbacks, and climate sensitivity. In V. Masson-Delmotte, P. Zhai, A. Pirani, S. L. Connors, C. Péan, et al. (Eds.), *Climate change 2021: The physical science basis. Contribution of working Group I to the sixth assessment report of the intergovernmental panel on climate change* (pp. 923–1054). Cambridge University Press. https://doi.org/10.1017/9781009157896.009

Jäger, H., & Wege, K. (1990). Stratospheric ozone depletion at northern midlatitudes after major volcanic eruptions. *Journal of Atmospheric Chemistry*, *10*(3), 273–287. https://doi.org/10.1007/BF00053863

Junge, C. E., Chagnon, C. W., & Manson, J. E. (1961). Stratospheric aerosols. *Journal of Meteorology*, *18*(1), 81–108. https://doi.org/10.1175/1520-0469(1961)018<0081:SA>2.0.CO;2

Junge, C. E., & Manson, J. E. (1961). Stratospheric aerosol studies. *Journal of Geophysical Research*, *66*(7), 2163–2182. https://doi.org/10.1029/JZ066i007p02163

Kalnajs, L. E., & Deshler, T. (2022). A new instrument for balloon-borne *In Situ* aerosol size distribution measurements, the continuation of a 50 year record of stratospheric aerosols measurements. *Journal of Geophysical Research: Atmospheres*, *127*(24). e2022JD037485. https://doi.org/10.1029/2022JD037485

Kräuchi, A., Philipona, R., Romanens, G., Hurst, D. F., Hall, E. G., & Jordan, A. F. (2016). Controlled weather balloon ascents and descents for atmospheric research and climate monitoring. *Atmospheric Measurement Techniques*, *9*(3), 929–938. https://doi.org/10.5194/amt-9-929-2016

Kremser, S., Thomason, L. W., von Hobe, M., Hermann, M., Deshler, T., Timmrech, C., et al. (2016). Stratospheric aerosol- Observations, processes, and impact on climate. *Reviews of Geophysics*, *54*(2), 278–335. https://doi.org/10.1002/2015RG000511

Li, Y., Dykema, J., Deshler, T., & Keutsch, F. (2021). Composition dependence of stratospheric aerosol shortwave radiative forcing in northern midlatitudes. *Geophysical Research Letters*, *48*(24), e2021GL094427. https://doi.org/10.1029/2021GL094427

Massie, S. T., Deshler, T., Thomas, G. E., Mergenthaler, J. L., & Russel, J. M., III. (1996). Evolution of the infrared properties of the Mount Pinatubo aerosol cloud over Laramie, Wyoming. *Journal of Geophysical Research*, *101*(D17), 23007–23019. https://doi.org/10.1029/96JD01991

Murphy, D. M., Froyd, K. D., Bourgeois, I., Brock, C. A., Kupc, A., Peischl, J., et al. (2021). Radiative and chemical implications of the size and composition of aerosol particles in the existing or modified global stratosphere. *Atmospheric Chemistry and Physics*, *21*(11), 8915–8932. https://doi.org/10.5194/acp-21-8915-2021

NASA Earth Observatory. (2021). Retrieved from https://earthobservatory.nasa.gov/images/148190/tracking-la-soufrieres-plume

Peterson, D. A., Campbell, J. R., Hyer, E. J., Fromm, M. D., Kablick, G. P., III, Cossuth, J. H., & DeLand, M. T. (2018). Wildfire-driven thunderstorms cause a volcano-like stratospheric injection of smoke. *NPJ Climate and Atmospheric Science*, *1*(30), 38. https://doi.org/10.1038/s41612-018-0039-3

Quenzel, H. (1969). Influence of refractive index on the accuracy of size determination of aerosol particles with light-scattering aerosol counters. *Applied Optics*, *8*(1), 165–169. https://doi.org/10.1364/ao.8.000165

Robock, A. (2000). Volcanic eruptions and climate. *Reviews of Geophysics*, *38*(2), 191–219. https://doi.org/10.1029/1998RG000054

Rollins, A. W., Thornberry, T. D., Atlas, E., Navarro, M., Schauffler, S., Moore, F., et al. (2018). SO_2 observations and sources in the western Pacific tropical tropopause region. *Journal of Geophysical Research: Atmospheres*, *123*(23), 13549–13559. https://doi.org/10.1029/2018JD029635

Russell, P. B., & Hamill, P., (1984). Spatial variation of stratospheric aerosol acidity and model refractive index: Implications of recent results. *Journal of the Atmospheric Sciences*, *41*(11), 1781–1790. https://doi.org/10.1175/1520-0469(1984)041<1781:SVOSAA>2.0.CO;2

Russell, P. B., Livingston, J. M., Pueschel, R. F., Bauman, J. J., Pollack, J. B., Brooks, S. L., et al. (1996). Global to microscale evolution of the Pinatubo volcanic aerosol derived from diverse measurements and analyses. *Journal of Geophysical Research*, *101*(D13), 18745–18763. https://doi.org/10.1029/96JD01162

Solomon, S., Daniel, J. S., Neely, R. R., Vernier, J.-P., Dutton, E. G., & Thomason, L. W. (2011). The persistently variable "Background" stratospheric aerosol layer and global climate change. *Science*, *333*(6044), 866–870. https://doi.org/10.1126/science.1206027

Solomon, S., Portmann, R., Garcia, R. R., Thomason, L., Poole, L. R., & McCormick, M. P. (1996). The role of aerosol variation in anthropogenic ozone depletion at northern midlatitudes. *Journal of Geophysical Research*, *101*(D17), 6713–6727. https://doi.org/10.1029/95JD03353

Steele, H. M., & Hamill, P. (1981). Effects of temperature and humidity on the growth and optical properties of sulphuric acid-water droplets in the stratosphere. *Journal of Aerosol Science*, *12*(6), 517–528. https://doi.org/10.1016/0021-8502(81)90054-9

Sterling, C. W., Johnson, B. J., Oltmans, S. J., Smit, H. G. J., Jordan, A. F., Cullis, P. D., et al. (2017). Homogenizing and estimating the uncertainty in NOAA's long-term vertical ozone profile records measured with the electrochemical concentration cell ozonesonde. *Atmospheric Measurement Techniques*, *11*(6), 3661–3687. https://doi.org/10.5194/amt-11-3661-2018

Thomason, L. W., Kent, G. S., Trepte, C. R., & Poole, L. R. (1997). A comparison of the stratospheric aerosol background periods of 1979 and 1989-1991. *Journal of Geophysical Research*, *102*(D3), 3611–3616. https://doi.org/10.1029/96JD02960

Wang, H. J. R., Damadeo, R., Flittner, D., Kramarova, N., Taha, G., Davis, S., et al. (2020). Validation of SAGE III/ISS solar occultation ozone products with correlative satellite and ground-based measurements. *Journal of Geophysical Research: Atmospheres*, *125*(11). https://doi.org/10.1029/2020JD032430

World Meteorological Organization. (1957). Definition of the tropopause. *Bulletin of the World Meteorological Organization*, *6*, 136–137.

Yu, P., Toon, O. B., Bardeen, C. G., Zhu, Y., Rosenlof, K. H., Portmann, R. W., et al. (2019). Black carbon lofts wildfire smoke high into the stratosphere to form a persistent plume. *Science*, *365*(6453), 587–590. https://doi.org/10.1126/science.aax1748